

Nanoscale

Accepted Manuscript



This is an *Accepted Manuscript*, which has been through the Royal Society of Chemistry peer review process and has been accepted for publication.

Accepted Manuscripts are published online shortly after acceptance, before technical editing, formatting and proof reading. Using this free service, authors can make their results available to the community, in citable form, before we publish the edited article. We will replace this *Accepted Manuscript* with the edited and formatted *Advance Article* as soon as it is available.

You can find more information about *Accepted Manuscripts* in the [Information for Authors](#).

Please note that technical editing may introduce minor changes to the text and/or graphics, which may alter content. The journal's standard [Terms & Conditions](#) and the [Ethical guidelines](#) still apply. In no event shall the Royal Society of Chemistry be held responsible for any errors or omissions in this *Accepted Manuscript* or any consequences arising from the use of any information it contains.

ARTICLE

Nanotextured stainless steel for improved corrosion resistance and biological response in coronary stenting

Cite this: DOI: 10.1039/x0xx00000x

Received 00th January 2012,
Accepted 00th January 2012

DOI: 10.1039/x0xx00000x

www.rsc.org/

Chandini C. Mohan†, Anupama Prabhath†, Aleena Mary Cherian, Sajini Vadukumpully, Shantikumar V. Nair, Krishnaprasad Chennazhi and Deepthy Menon*

Nanosurface engineering of metallic substrates for improved cellular response is a persistent theme in biomaterials research. The need to improve the long term prognosis of commercially available stents has led us to adopt a ‘polymer-free’ approach which is cost effective and industrially scalable. In this study, 316L stainless steel substrates were surface modified by hydrothermal treatment in alkaline pH, with and without the addition of a chromium precursor, to generate a well adherent uniform nanotopography. The modified surfaces showed improved hemocompatibility and augmented endothelialization, while hindering the proliferation of smooth muscle cells. Moreover, they also exhibited superior material properties like corrosion resistance, surface integrity and reduced metal ion leaching. The combination of improved corrosion resistance and selective vascular cell viability provided by nanomodification can be successfully utilized to offer a cell-friendly solution to the inherent limitations pertinent to bare metallic stents.

Introduction

Austenitic Stainless Steel (SS) is widely employed biomaterial with applications in cardiovascular, orthopedic, dental, and craniofacial implants.^{1,2} However, bare metallic SS stents are afflicted by *in situ* corrosion, acute thrombosis and neointimal hyper proliferation, leading to in-stent restenosis and risk of myocardial infarction.³ Reports have shown that sub-lethal concentrations of metallic ions from corrosion products could exacerbate the pro-inflammatory and fibrotic reactions, leading to narrowing of the arterial lumen.^{4,5} In order to address the limitations of bare metallic stents (BMS), the scientific community offers various approaches such as coating with biocompatible materials like gold, diamond like carbon, silica and hydroxyapatite, surface immobilization of biological moieties like heparin as well as the use of biodegradable and drug eluting stents.⁶⁻⁹ Biological coatings are allied with inherent limitations of instability, leading to aberrant vascular healing.¹⁰ Biodegradable metallic stents such as those based on Mg or Fe undergo rapid degradation in physiological environment.¹¹ This degradation causes tissue inflammation and loss of mechanical integrity, leading to a negative remodeling of the treated arteries, making these stents less viable for clinical use.^{12,13} Drug eluting stents (DES) are arguably the best feasible alternative to BMS. However, anti-proliferative drugs employed in DES impede the recovery of a functional endothelium due to its cytotoxicity, resulting in delayed endothelialization, bare stent exposure and consequently late stent thrombosis.¹⁴ Moreover, the acute and

delayed hypersensitivity due to polymeric delamination results in an additional risk to the outcome of DES implantation.¹⁵ For obtaining better *in vivo* response for BMS, ion implantation with metals like Ti and Ta has been adopted.¹⁶ These modifications impart improved corrosion resistance by providing a barrier metal oxide layer. However, the high energy ion bombardment could result in an increased surface damage and thereby higher probability of material failure.¹⁷ In recent years, nanotechnology has emerged as an innovative option by endorsing surface texturing for promoting application-specific cellular response.¹⁸ Previous research by our group has demonstrated the effectiveness of TiO₂ nanostructures in promoting the growth of vascular endothelial cells, while hindering the over proliferation of smooth muscle cells and platelets *in vitro*.¹⁹ Likewise, these nanostructures also provided improved osteoblast response *in vitro*²⁰ and *in vivo*.²¹ Moreover, nanostructuring of implant materials have also found to impart surfaces with superior electrochemical and mechanical properties, irrespective of the metallic substrate.^{22,23} Works carried out by Xhang and co-workers demonstrated enhanced corrosion behavior for nanocrystalline Zr compared to the microcrystalline form.²⁴

In the present study, we have adopted a cell-friendly approach of nanosurface modification of 316L SS to entail the dual features of non-destructive cellular modulation with superior corrosion resistance and stability through alkaline hydrothermal processing. The possibility of achieving higher chromium to iron (Cr/Fe) ratio on SS surface by hydrothermal processing

with and without the use of a chromium source has been explored for improved corrosion resistance and mechanical integrity. The influence of nanotexturing on hemocompatibility and vascular cell behavior was also assessed as a part of the biocompatibility evaluation. This study is a primary effort in exploring a simple thermo-chemical surface modification of SS for generating nanocrystalline structures for providing selective vascular cell response, to serve as a viable option for drug eluting strategies in coronary stenting.

Experimental section

Materials and methods

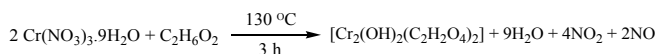
Medical grade 316L stainless steel plates with composition (wt%) of 64% Fe, 17% Cr and 13.6% Ni as the major elements and diameter of 14 mm was purchased from M/s Jayon Surgicals Pvt Ltd, India. SiC paper of grit size ranging from 120 to 1200 and alumina suspension of 1 and 0.05 microns used for polishing the plates was purchased from Buehler Inc. USA. Sulfuric acid (H₂SO₄) and hydrogen peroxide (H₂O₂) used to make the Piranha solution was purchased from Merck India Pvt Ltd, India. Other chemicals used in the experiment include Sodium hydroxide (NaOH) (Extra pure, Sigma), Chromium Nitrate (Cr(NO₃)₃·9H₂O) (Spectrochem Pvt Ltd, India), Ethylene glycol and Acetone (Merck Pvt Ltd, India). All chemicals were used as received, without any further purification.

Pre-treatment of SS for hydrothermal reaction

Prior to hydrothermal treatment, the SS samples were mechanically polished progressively using SiC papers (of grit sizes 600, 800 and 1200) and thereafter using alumina suspension of 1 and 0.05 microns in a polishing machine (Buehler Beta Grinder Polisher, USA). After each polishing step, the samples were ultrasonicated (Misonix Inc, USA) in acetone, followed by distilled water for typically 10 min. The cleaned and air dried samples were later subjected to piranha treatment (3:1 ratio of H₂SO₄:H₂O₂). This is to remove redundant organics and provide a very clean surface as well as to activate the surface prior to hydrothermal treatment.²⁵ The piranha etched samples were washed thoroughly under ultrasonication in excess of milliQ water for 10 min and dried in a hot air oven set to 40°C.

Preparation of chromium precursor

In an attempt to surface modify SS with enriched Cr content, an approach of hydrothermal treatment in presence of a chromium precursor was adopted. For this, a chromium precursor complex which acts as a source for chromium oxide was prepared as follows.²⁶



The chromium precursor synthesis was carried out in a 3-necked round bottom flask. Cr(NO₃)₃ (0.03 M) was completely dissolved in ethylene glycol (0.13 M) at a ratio of 2:1 under reflux condensation at 130°C for 3 h. The reaction product obtained after cooling was purified to remove all by-products by repeated washing with excess of acetone, filtered and dried

at 60°C for 2 h in air and stored in hot air oven for further experiments.

Hydrothermal treatment of pre-treated SS samples

Hydrothermal treatment of pre-treated SS samples was carried out in an alkaline medium (pH ~13) at varied conditions of temperature, molar concentration and reaction time in an indigenously fabricated high temperature furnace (Hi Heat Furnaces, Cochin) equipped with a programmable temperature controller (Shinko Technos Co., Ltd, Japan). Samples were immersed in 40 mL of NaOH solution (0.5, 1, 5, 10 M) taken in a teflon vessel and placed inside a stainless steel autoclave which was subjected to hydrothermal treatment (referred to as PHT) in a furnace under various temperature (150-500°C) and reaction time (2, 4, 5, 8, 9 and 12h). Likewise, hydrothermal processing of SS substrates was also carried out under same processing conditions with the addition of 0.001 wt% Cr precursor (referred to as PHT Cr). After the reaction, the samples were collected and sonicated for 10 min, washed and air dried.

Characterization techniques

The morphology of the treated samples was examined using scanning electron microscope (JEOL 6490L Analytical scanning electron microscope SEM, Japan). Energy dispersive analysis was performed to quantify the surface percentage composition using the EDAX attached to the SEM. XPS analyses (Axis Ultra DLD, Kratos Analyticals, UK) were carried out to assess the surface chemistry of the samples. Crystallinity was analyzed using an X-ray diffractometer (X'Pert Pro, PANalytical) fitted with a Cu Kα (λ = 1.541 Å) in the range 10° to 80° at a step size of 0.05°. The JCPDS database was utilized in phase identification. Surface roughness of the bare and nanomodified samples was analyzed by stylus profilometry using a surface profiler (Veeco Dektak 150 Profiler, USA). By summing the deviations from the centerline and dividing the number of data points along a length of 500 μm (n=5), the average roughness of the samples was determined and interpreted.

In vitro corrosion studies

Corrosion resistance of the two surface modified samples was analyzed in comparison to non-treated, control SS using an electrochemical work station (Autolab, Metrohm). Open circuit potential (OCP) analysis was done for **30 min** in Phosphate Buffered Saline (PBS) at a pH of 7.4 to attain a steady state condition. Linear sweep voltammetry experiments were performed at a scan rate of **0.5 mVs⁻¹** in PBS using an electrochemical cell, which consisted of a platinum counter electrode, and an Ag/AgCl reference electrode. The specimen area exposed to the electrolyte solution was 1 cm² and the potential range was set between **-1.0 and +1.0 V**.²⁷ The corrosion potential (E_{corr}) and corrosion current density (i_{corr}) were determined by Tafel extrapolation method using Tafel tool bar software in Origin Lab, version 9.²⁸

Static immersion tests for ion release analysis

Surface modified SS samples were subjected to a static immersion test for ion release analysis in comparison to bare SS. The samples were immersed in a solution containing 10 mL

PBS maintained at pH 7.4, with 100 μL of antibiotic Pen Strep and kept in shaker incubator maintained at 37°C. The percentage of ion release was analyzed by inductively coupled plasma atomic emission spectroscopic (ICP-AES) analysis after 1, 14, and 28 days to quantify the time dependent release of Ni^{2+} , Cr^{2+} and Fe^{3+} ions from various samples.²⁹ Untreated bare polished SS was maintained as the control, with a bare sample coated with the epoxy resin on both sides (to calculate any ion release from the resin) kept as the blank.

Nanoindentation and nanoscratch analyses

The hardness and modulus of elasticity of modified substrates were compared with respect to the bare polished SS substrate by a nanoindenter (TI-900, Hysitron Inc., USA) with a diamond Berkovich tip (200nm radius) using Oliver Pharr nanoindentation method with special load and displacement control properties. A constant load of 10 mN was retained for 10 s and the corresponding load displacement curve was plotted to elucidate the mechanical properties of the samples.³⁰ The scratch resistance, integrity and average roughness of the modified surfaces were deduced from a nanoscratch test performed using the same nanoindenter. A progressive load of 0.1 μN - 10 mN was applied to the sample and the scratch distance was set to 10 $\mu\text{m}/\text{min}$. The distance progressed by the tip without failure signifies the scratch resistance of the film. The load at which the failure occurred was determined from the plot of force vs displacement that corresponds to the 'critical load'.

Hemocompatibility studies

To evaluate the blood compatibility of surface modified SS samples, interactions with various blood components were assessed. 30 mL of whole blood was drawn from healthy volunteers in sodium citrate containing vials. The samples were incubated with 2 mL whole blood for 1 h with mild shaking at 37°C. Positive and negative controls were maintained for each of the experiments.

Hemolysis assay

The plasma hemolytic character of the modified substrates was analyzed spectrophotometrically (UV-1700, Shimadzu) with reference to unmodified SS as control by Soret band absorption of free hemoglobin at 415 nm. The whole blood after treatment with the substrates was centrifuged at 4500 rpm for 15 min and platelet poor plasma (PPP) was isolated. The absorbance of diluted PPP containing 0.01% sodium bicarbonate (1:10) was measured at 380, 415 and 450 nm. Plasma hemoglobin was estimated to calculate the percentage of hemolysis (Eq. 1) by the equation.

$$\text{Amount of plasma free - hemoglobin (mg / dL)} = \frac{2 \times A_{415} - (A_{380} + A_{450}) \times 1000 \times \text{Dilution factor}}{(E \times 1.655)}$$

(Eq 1)

A represents the absorbance. A_{415} is the Soret band based absorption of hemoglobin, A_{380} and A_{450} are the correction factors applied for uroporphyrin, another pigment whose absorption falls in the same wavelength range. E is molar absorptivity value of oxyhemoglobin at 415 nm which is 79.46. 1.655 is the correction factor applied due to the turbidity of plasma sample. The percentage hemolysis was calculated as:

$$\% \text{ Hemolysis} = \frac{\text{Plasma Hb value of sample}}{\text{Total Hb value of blood}}$$

0.9 % saline and 1% Triton X-100 served as negative and positive controls, respectively in this experiment.

Coagulation studies

To analyze if the surface modified samples induced any alterations in the blood coagulation profile, the samples were incubated with whole blood for 2 h. Post incubation, the blood was collected and centrifuged to extract PPP. This extract was employed in coagulation assays to assess the influence of the material in activating the extrinsic and intrinsic pathways of coagulation using the coagulation analyzer. Prothrombin time (PT), activated partial thromboplastin time (APTT) and thrombin time (TT) were measured using the reagent kits (STA Neoplastine CL, CK Prest and Thrombin Time) from Diagnostica Stago (France) following manufacturer's protocol.

Platelet aggregation

Interactions of platelets with the modified substrates were studied using a platelet aggregation assay. Whole blood was incubated on the samples under static conditions at room temperature for 1 h. Post incubation, blood was collected and platelet count was analyzed using hematology analyzer (Cell Dyn 3700, Abbott, USA). PBS and adenosine dihydrogen phosphate (ADP) served as negative and positive controls, respectively. The platelet count values obtained were plotted.³¹

Cell culture and cell viability assay

Human umbilical vein endothelial cells (HUVEC) and Vascular smooth muscle cells (SMCs) were isolated from umbilical cord collected from voluntary donors with approval of the Institutional Ethical Committee of Amrita Institute of Medical Sciences, Kochi, adopting the protocol reported by Jaffe et al.³² The cells used for the experiment were at the 3rd or 4th passage, maintained in Iscove's Modified Dulbecco's Media (IMDM) growth medium supplemented with 20% FBS and Endothelial cell growth supplement (ECGS, Sigma, USA) for their normal growth and viability. Similarly, smooth muscle cells were also cultured in platelet derived growth factor (PDGF) supplemented 20% IMDM growth medium upto 4th and 5th passage before being used for the experiments. Cell viability on nanomodified SS was assessed by Alamar Blue assay and compared with that of control polished bare SS. HUVEC cells were seeded on the SS plates at a density of 1.6×10^4 cells/ cm^2 . After incubation for the required study period of 24, 72 and 120 h, SS samples were washed with PBS to remove non-adherent cells. The cells adherent on the substrate were incubated with Alamar blue (Invitrogen Life Sciences, USA) for 6 h and the color change was quantitatively recorded by measuring the optical density using a microplate spectrophotometer (Model: BioTek Powerwave XS, USA) at 570 nm, with 600 nm set as the reference wavelength. Similar study was done with SMCs at the same seeding density. All the experiments were done in triplicate.

Cell Morphological analysis by fluorescent staining

SS samples were cultured individually with HUVEC and SMCs at a cell density of 1.6×10^4 cells/ cm^2 in 20% IMDM for a period

of 5 days, followed by fixation in 4% paraformaldehyde in PBS for imaging. Consequently, the cells were permeabilized with 0.5 % Triton X-100 in PBS for 5 min and the non-specific binding sites were blocked with 1% FBS in PBS for 15 min. Further, the cells were stained using Texas red conjugated Phalloidin (Molecular probes, Invitrogen Life Sciences, USA) for 60 min at room temperature to visualize the actin filament assembly. The samples were further counter stained with DAPI (Molecular probes, Invitrogen Life Sciences, USA) to image the nucleus.

Statistical analysis

All quantitative results were carried out in triplicates and are expressed as mean \pm SD. The statistical analyses were performed using one-way ANOVA, followed by Tukey's post-hoc tests by means of OriginLab software, USA (OriginPro8). $p < 0.05$ were considered statistically significant. * $p < 0.05$ and ** $p < 0.01$ indicate statistical significance with respect to polished control SS. # $p < 0.05$ and ## $p < 0.01$ represent statistical significance between the two nanosurfaces compared, viz., PHT and PHT Cr

Results and discussion

Nanosurface modification of SS

Hydrothermal technique has been established to create a highly crystalline surface texture at the nanoscale, with its architecture being dictated by the experimental parameters such as temperature, pH, time, etc. This technique involves the activation energy dependent dissolution, primary-secondary nucleation and diffusion controlled particle growth of the elements which are relatively insoluble under normal conditions.³³ Our group has already proven that such a treatment in alkaline pH can induce nanotopographical alterations on metallic Ti, with temperature and concentration of NaOH being the key determinants.¹⁹ In this study, uniform nanostructures were developed on the surface of SS by direct hydrothermal technique under alkaline conditions as well as with the addition of a chromium precursor. Fig. 1A represents the SEM images of surface modified SS at different magnifications (Ai, Aii, Aiii) subsequent to direct hydrothermal processing in 0.5 M NaOH at 250°C for 5 h (PHT) depicting nanosized pyramidal structures having well defined faceted morphology.

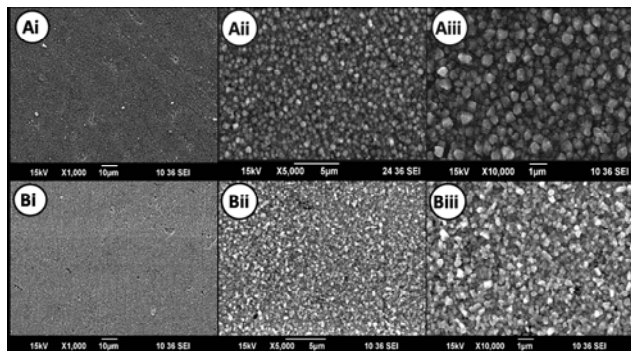


Fig. 1 SEM of surface modified SS samples at different magnifications by (A) direct hydrothermal treatment (PHT) and (B) in presence of chromium precursor (PHT Cr)

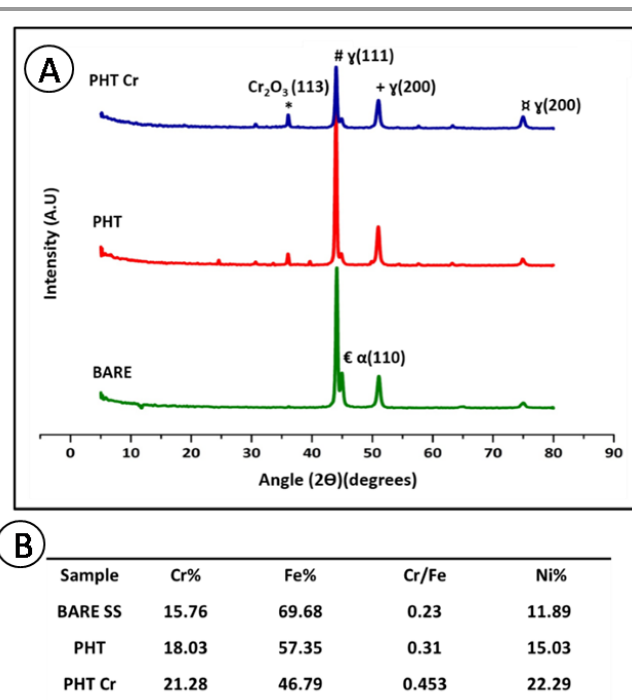


Fig. 2 (A) XRD patterns of bare and modified SS samples with the representations implying the following: # $\gamma(111)$, + $\gamma(200)$ * $\text{Cr}_2\text{O}_3(113)$ and $\alpha \alpha(110)$ and (B) Atomic percentages of the major elements (Fe, Cr, Ni) on bare and modified SS.

Samples subjected to hydrothermal processing in NaOH under identical conditions, but with the addition of 0.001 wt% Cr precursor (PHT Cr) also revealed a dense, uniform nanotexture with submicron sized pyramidal structures as seen in Fig. 1B (Bi, Bii, Biii). The average roughness of the nanotextured oxide layer on SS deduced through surface profilometry was found to be 0.41 and 0.18 nm for PHT and PHT Cr, respectively. X-ray diffraction analysis was used to decipher the differences in crystallinity and phase change induced by nanotexturing of SS. As clearly evident from Fig. 2A, untreated bare SS depicted the characteristic peaks of face centered cubic γ -austenitic phases, viz., (111), (200) and (220).³⁴ Moreover, the body centered cubic (BCC) α -ferrite phase (110) is present adjacent to the γ -austenitic phase at a 2θ value of 44.5°. Upon direct hydrothermal treatment, the γ -austenitic phase (111) was intensified, while the BCC α -ferrite phase got diminished. Additionally, a new peak appeared at 35.5° which signify the development of the oxide phase of Cr, viz., Cr_2O_3 . In contrast, PHT Cr samples showed a significantly reduced intensity for the γ -austenitic phase at (111) as well as the BCC α -ferrite phase, with the Cr_2O_3 peak retained at 35.5°.³⁵ This clearly implies that hydrothermal treatment, both direct and precursor mediated, resulted in the formation of a chromium-rich oxide layer on SS, indicating the surface passivation of the modified samples.

This was further substantiated with the composition analysis by EDAX. Table in Fig. 2B depicts the atomic percentages of the SS alloy components, viz., Cr, Fe and Ni, on bare and modified SS. As evident from the table, there is a significant improvement in the Cr/Fe ratio from 0.23 for bare SS to 0.31 for PHT and 0.45 for PHT Cr samples. This enhanced Cr/Fe ratio for the precursor treated sample confirms the speculation that additional chromium fortifies the SS surface with a passive

layer. Moreover, the piranha treatment removes the native oxide layer and incorporates hydroxyl groups, which could further improve the nucleation of chromium ions, which was confirmed by the XRD results.³⁶ However, the percentage of Nickel content was also found to be elevated as evident from the tabulation. Whether these Ni ions were present in their free or bound state was confirmed by XPS as detailed below.

Quantitative surface chemical analysis

Surface compositional analysis of the hydrothermally treated SS samples was assessed by XPS. Figs. 3A-D depict the high resolution XPS spectra of Cr 2p, Fe 2p, Ni 2p and O 1s from the wide spectra for all the samples. The chromium oxide and hydroxide peaks of Cr 2p at 575 and 586 eV³⁵, respectively were observed in PHT Cr, while the intensity was reduced for the sample subjected to direct hydrothermal treatment (PHT) (Fig. 3A). The elevated intensity for the precursor mediated SS sample suggests that the thickness of the chromium oxide layer has improved considerably after hydrothermal treatment in presence of a chromium precursor. The high resolution XPS spectra of Fe 2p (Fig. 3B) indicates that the metallic peak of iron (Fe 2p) at a binding energy of 702 eV was absent in the treated substrates. Instead, a high intensity peak appeared at a binding energy of 711.5 eV on the hydrothermally modified samples, suggestive of the fact that free iron was converted to its hydroxide state.³⁷ The Ni 2p spectra shown in Fig. 3C illustrate the presence of Ni in its bound state as Ni(OH)₂ at a binding energy of 857 eV, with a significant shift from its free state at 853 eV.³⁷ The coherent peaks of O 2p in the range of 530-531 eV for all the samples denote that the surface layer is composed of metallic oxides and hydroxides of iron and chromium respectively.³⁸ Thus, XPS analyses clearly revealed that nanotextured SS has a surface passivation layer rich in chromium and iron in their oxide form, with nickel occurring in hydroxide form.

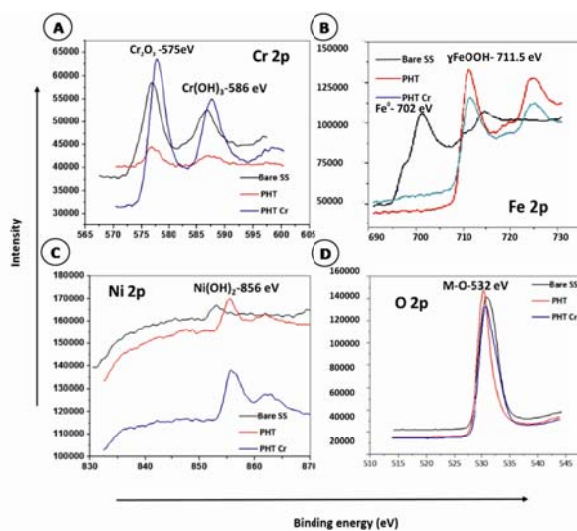
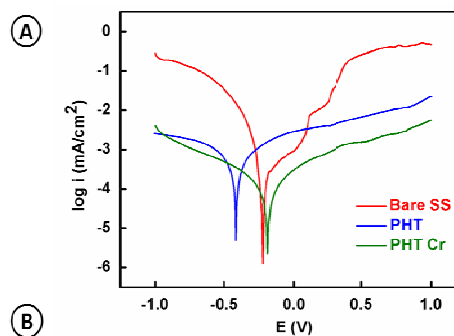


Fig. 3 Surface compositional analysis by XPS depicting the high resolution spectra of (A) Cr 2p (B) Fe 2p (C) Ni 2p and (D) O 2p for bare and modified SS.

In vitro corrosion studies

The corrosion behavior of the samples were characterized by potentiodynamic polarization in simulated body conditions and the standard Tafel plot extrapolation was done for deriving the corrosion parameters. Fig. 4A shows the compiled Tafel plots of bare and the modified substrates and Fig. 4B provides a tabulation of its corrosion parameters. **In comparison to bare SS, there is a shift in the potential of the direct HT treated sample towards the cathodic region, leading to a decrease in the corrosion potential (-0.386 V). However, in contrast to bare SS, the corrosion current density decreased to a value of 1.096 $\mu\text{A}/\text{cm}^2$ resulting in a milder corrosion rate of 0.011 mmpy. On the contrary, the precursor mediated sample showed a positive shift towards the anodic region with an E_{corr} value of -0.198 V and a lower corrosion current density of 0.173 $\mu\text{A}/\text{cm}^2$, which suggests an improved corrosion behavior of the surface. Further, the increase in the anodic curve of bare SS represents its tendency for breakdown, attributed to active corrosion due to localized pitting at higher potentials.^{39,40} In contrast, the hydrothermally treated samples showed a steady increase in anodic current without any rapid rise. Thus, apart from the uniformity in surface topography attained by the hydrothermal treatment, polarization characteristics of the samples displayed significant resistance to corrosion in a simulated body environment.** This characteristic pattern of corrosion resistance exhibited by the treated substrates could be well attributed to the intrinsic formation of a surface chromium oxide film with increased Cr/Fe ratio as confirmed from the EDAX and XPS analysis. Moreover, the presence of a chromium precursor in the hydrothermal medium helped to alter the surface chemistry as well as topographical cues on SS. A chromium rich layer, with the elements (Cr, Fe and Ni) held in their bound state was confirmed by XRD and XPS. In the Tafel plot, the anodic shift coupled with the reduction in corrosion current density and corrosion rate supported the spectroscopic analysis, revealing better corrosion resistance for a chromium rich layer.



Sample	E_{corr} (V)	I_{corr} ($\mu\text{A}/\text{cm}^2$)	CR (mmpy)
Bare SS	-0.209	4.875	0.051
PHT	-0.386	1.096	0.011
PHT Cr	-0.198	0.173	0.002

Fig. 4 (A) The standard Tafel plot of bare and modified SS substrates (B) Tabulation of the corrosion parameters

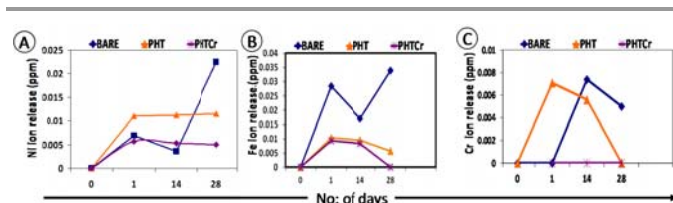


Fig. 5 Ion release profiles of (A) Nickel (B) Iron and (C) Chromium ions from bare and surface modified SS samples in PBS at different durations measured by ICP-AES

Ion release studies

The metallic ion release profiles from bare and surface modified SS substrates were carried out in PBS and analyzed using ICP-AES for a period of 4 weeks, with a 14 day interval between each reading. Fig. 5 shows the amount of Ni (A), Fe (B) and Cr (C) ions released respectively from bare SS, PHT and PHT Cr samples. The release profiles of Ni ions showed a sharp enhancement in the ion concentration for bare SS as against that of hydrothermally modified samples that measured a low Ni ion concentration throughout the tested time period. Likewise, the concentrations of Cr as well as Fe ions leached into the medium were also substantially less for the precursor treated SS substrate in comparison to bare SS after duration of 28 days. All these can be attributed to the efficient surface passivation mediated by the hydrothermal treatment with and without the chromium precursor, wherein the ions are retained in their bound state on the metallic surface.

Nanoindentation and nanoscratch testing

The nanoindentation and scratch tests were carried out to determine the integrity of the coating layer onto the substrate. The full cycle load-displacement curves for the samples at a maximum load of 10 mN for 10 s indentation are depicted in Fig. 6A.

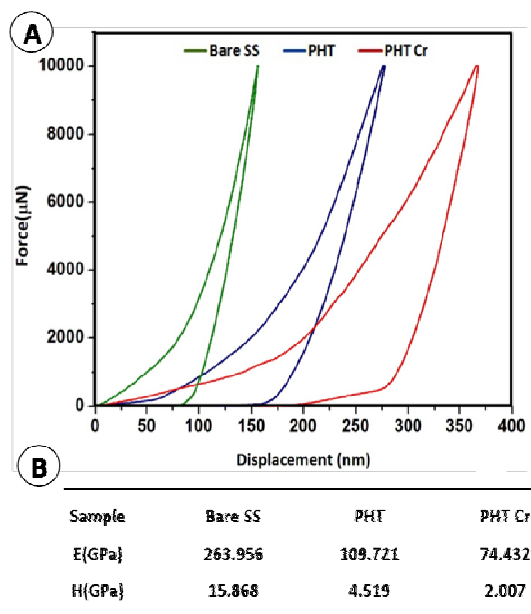


Fig. 6 (A) Load-displacement curves of bare and surface modified SS samples and (B) Table depicting the modulus of elasticity (E) and hardness (H) of the measured surfaces

The key features to be noted in this graphical representation are the maximum penetration depth and the unloading recovery of the surface being examined. It is important to mention that in the load-displacement curves of SS and surface modified SS shown in Fig. 6A, no discontinuities or local perturbations were observed in the load-controlled experiments, which normally signify any characteristic energy absorbing or energy releasing events (delamination, cracks) occurring beneath the indenter tip. The bare SS loading-unloading curve showed a relatively enhanced elastic behavior, while PHT and PHT Cr depicted similar trends, with response curves displaced to the right. The PHT Cr sample showed a relatively higher penetration compared to bare SS and PHT, which is more evident in the unloading pattern. The same trend was noticeable in the tabulated values of elasticity and hardness represented in Fig 6 B, wherein bare SS showed very high modulus of elasticity as well as hardness values. Amongst the nanosurfaces, PHT Cr showed a comparatively reduced elastic behavior, while PHT portrayed the characteristic features of a ductile solid.

Figs. 7A and B depict the representative 2D topographical *in situ* SPM images obtained on PHT and PHT Cr samples, respectively after a 10 mN ramping force nanoscratch test. The mechanical integrity of the surface coating was assessed using this test, wherein the failure events such as delamination, cracks or debonding at film/substrate interface becomes clearly evident in the SPM image during scratching. Herein in Fig. 7A and B, the SPM images demonstrated no evidence of cracking or delamination of the surface oxide layer for the modified SS substrates along their scratch length. Adhesion of surface coating to the substrate was also deduced from the critical load value L_c in the force-displacement curve represented in Figs 7 C and D, obtained during the nanoscratch experiment. Among the nanosurfaces compared, PHT exhibited a relatively higher L_c value of 9.9 mN and a longer scratch distance (5.4 μm) compared to PHT Cr which showed a lower L_c value of 2.9 mN.

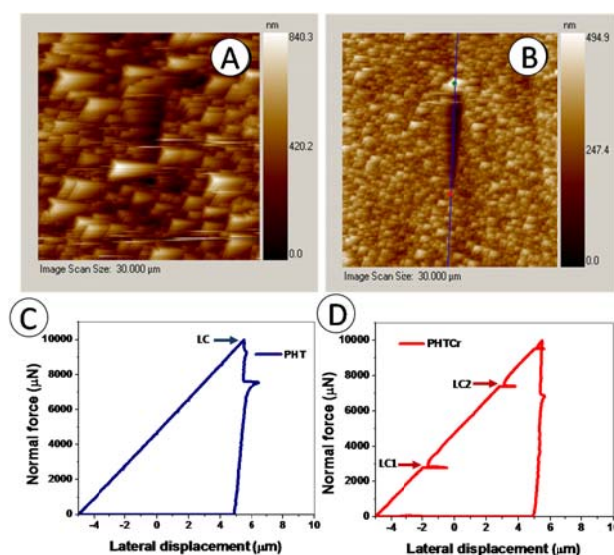


Fig. 7 SPM images of nanoscratches made on the surface of (A) PHT (B) PHT Cr. (C) and (D) represent the variation in normal force along the lateral tip displacement on PHT and PHT Cr respectively.

However, the SPM images clearly revealed no loss of integrity of the film, implying the adhesiveness and flexibility of nanomodified SS by resisting cracking/flaking upon progressive loading. The flexibility offered by the nanostructured oxide layer formed on SS is also reflected in their hardness and elasticity values (Fig. 6B).

Hemocompatibility studies

The proposed utility of the material as a blood contacting device is irrelevant without assessing its hemocompatibility profile. The primary concern is due to the immediate and continued contact of the material with blood upon implantation and throughout the lifetime of the material in the body. Surface modified SS samples were analyzed for their hemocompatibility using various assays such as coagulation assay, platelet count and hemolysis assay as detailed earlier.

Coagulation assay

Coagulation assays were done with the extracted PPP in order to evaluate the influence of the material in activating the extrinsic and intrinsic pathways of coagulation using a coagulation analyzer. Prothrombin time (PT), activated partial thromboplastin time (APTT) and Thrombin times (TT) were measured for the nanomodified SS samples in comparison to bare SS as shown in Fig. 8A. The nanosurface modified substrates showed a normal prothrombin time in the range of 11-17 s. Furthermore, TT and APTT values for the samples were in the standard range of 15-20 s and 25-39 s respectively, indicating that the nanotexturing approach did not induce the activation of any clotting factors in the coagulation cascade.

Platelet count

The extent of platelet aggregation is represented by analyzing the percentage reduction in platelet count on various treated surfaces. In Fig. 8B, the positive control (ADP treated blood) showed a prominent reduction in platelet count. This parameter is a precise indication of platelet aggregation on addition of ADP. In contrast, platelet aggregation was slightly lower on nanomodified SS surfaces than on bare SS, although the differences between PHT and PHT Cr were not statistically significant. The lowering of platelet aggregation is suggestive of the reduced activation of platelets on the nanomodified surface.

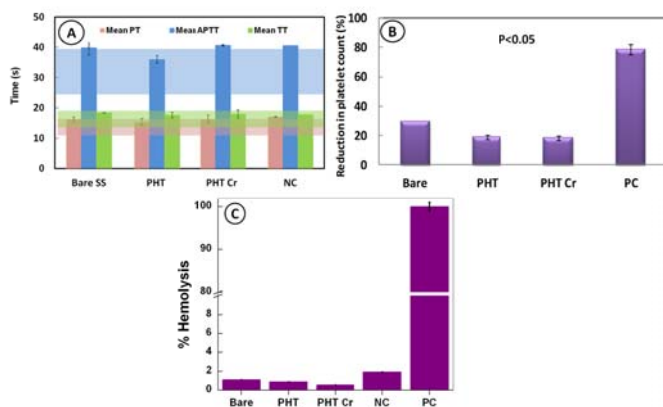


Fig. 8 (A) Mean clotting time (B) Reduction in platelet count and (C) Percentage hemolysis of the surface modified SS samples in comparison to unmodified SS.

Hemolysis Assay

Hemolysis assay was done to assess the influence of nanotexturing on the integrity of the formed elements of blood, especially with respect to RBC. Rupture of RBCs would leak free hemoglobin, intracellular components and thromboplastic substances into the plasma, which could in turn activate the clotting cascade, resulting in thrombus formation.⁴¹ The quantity of free hemoglobin in plasma was analyzed spectrophotometrically by the Soret band absorption. Fig. 8C shows the variations of hemolysis for all the substrates investigated. Our data satisfactorily proved that the novel surface has negligible adverse effect to the red blood cell integrity and function. The behavior was similar to the response exhibited by nanomodified titanium, implying that nanotexturing of metallic surfaces does not provoke any incompatibilities when in contact with blood.⁴²

Cell studies

Cell viability

In order to investigate the vascular cell compatibility of the surface, and its potential suitability for coronary stent applications, endothelial cells and SMCs were cultured independently on the substrates and tested for its viability at different time intervals by Alamar blue assay. Fig. 9A portrays the endothelial proliferation on the nanomodified SS substrates with respect to the bare counterpart which served as the control. Results indicate that, after day 1 the endothelial viability was significantly enhanced on nanosurfaces with progression of time (*p<0.05). While the endothelial cells primarily showed an increased uniform attachment on all the samples, SMCs showed a markedly reduced initial attachment (Fig. 9B). Both PHT and PHT Cr showed a substantially less smooth muscle cell viability after 3 and 5 days of *in vitro* culture compared to that on the bare SS (**p<0.01). Among the two nanosurfaces compared, PHT Cr exhibited better endothelial proliferation (#p<0.05) and a decreased smooth muscle cell viability than PHT (##p<0.01) after 5 days.

Thus, while the nanomodified substrates showed an overall improved endothelial cell response, it concurrently reduced the proliferation of SMCs when compared to bare SS. These results are also in accordance with the outcome on corrosion resistance and hemocompatibility, wherein PHT Cr showed improved performance than the other samples. Moreover, the superior endothelial cell viability of precursor mediated samples over SMCs shows the potential of the newly developed surface in providing a preferential cellular response. This can be attributed to the effect of nanotopographical profile in selectively mediating the adsorption, proliferation and growth of cells.

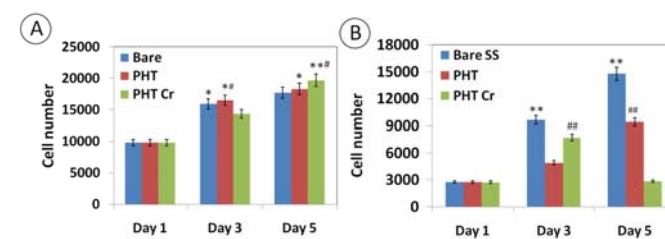


Fig. 9 Cell viability of (A) HUVEC and (B) SMC on the SS substrates at day 1, 3 and 5. *p<0.05 ** p<0.01 implies comparison of PHT and PHT Cr with bare SS; #p<0.05, ##p<0.01 represents comparison between PHT and PHT Cr.

Similar results on differential cell response for HUVECs and SMCs induced by nanotopography were observed by our own group on Ti surfaces as well, which was attributed to the differences in the focal adhesion mediated mechanotransduction pathways.¹⁹ Mechanical stimulations perceived by focal adhesions formed by cells on nanosurfaces can trigger the nucleus directly or indirectly and thereby influence various cellular events such as proliferation, migration, gene expression etc.^{43,44} Ceylan et al observed analogous results by developing a bioactive stent coating capable of promoting endothelialization while restricting the viability of SMCs.⁴⁵ Previous research by Webster et al has shown the enhanced endothelial cell function on rationally designed patterned titanium surfaces.⁴⁶ There is also a strongly reinforced argument that cells such as SMCs respond more effectively to submicrometric than to nanometric surfaces.⁴⁷

Bare SS stents continue to be used ubiquitously, despite the issue of pitting corrosion which causes toxic metal ion release, induces platelet activation and smooth muscle cell overproliferation leading to in-stent restenosis.⁴⁸ Endothelial cells which form the innermost lining of arteries play a critical role in maintaining vascular hemostasis, controlling smooth muscle cell proliferation and platelet activity.⁴⁹ Thus, a surface constructive to reestablishment of endothelium is the fundamental requirement for a vascular stent material.⁵⁰

Cell morphological analysis by fluorescence staining

The morphology of HUVECs and SMCs after incubation on the modified surfaces was also analyzed by fluorescent staining (Fig. 10). Here again, substantiating the results of Alamar Blue assay, HUVEC cells showed prominent cell growth and spreading on the nanomodified samples (Fig. 10 Bi, Bii and Ci, Cii) in comparison to bare SS (Fig. 10 Ai, Aii) at days 3 and 5. In contrast, SMC growth was significantly diminished on modified SS surfaces (Fig. 10 Biii, Biv and Ciii, Civ), while retaining a proliferative growth on bare SS (Fig. 10 Aiii, Aiv). A material capable of promoting endothelialization while restricting the proliferation of SMCs, coupled with improved mechanical and corrosion attributes would be an ideal substrate for vascular applications. Together, our results indicate that the precursor mediated surface modified SS surface would be an appropriate candidate for further studies as a coronary stent material.

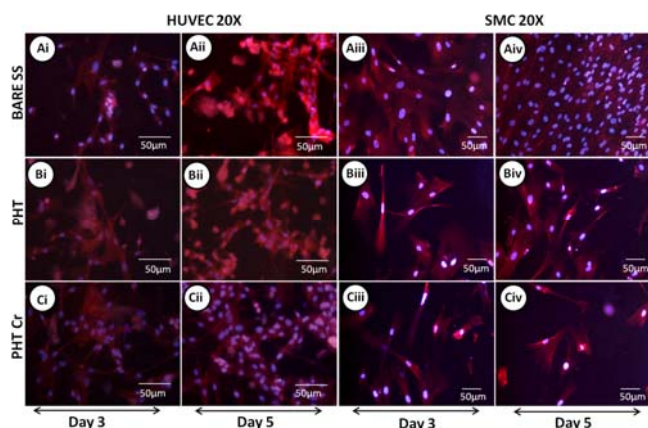


Fig. 10 Fluorescence staining of Actin (red) and DAPI (blue) for HUVECs and SMCs proliferating on (A) bare SS, (B) PHT and (C) PHT Cr surfaces at days 3 and 5.

A material capable of promoting endothelialization while restricting the proliferation of SMCs, coupled with improved mechanical and corrosion attributes would be an ideal substrate for vascular applications. Together, our results indicate that the precursor mediated surface modified SS surface would be an appropriate candidate for further studies as a coronary stent material.

Conclusions

The present study reports the development of an intrinsic, uniform nanotextured layer on SS substrates by simple oxidative processing using an alkaline hydrothermal technique in presence of a chromium precursor. The nanotopography was conducive in providing a surface milieu that selectively promoted endothelialization and hindered the over proliferation of SMCs and platelets. Moreover, it also provided improved corrosion resistance and mechanical stability, both of which are fundamental to the success of any metallic implant. These results provide exciting insights into the prospect of employing hydrothermal technique for nanosurface modifying SS stents. The dual triumph of improved corrosion resistance and selective vascular cell viability of the novel surfaces can be successfully maneuvered to provide a long term solution to the inherent problem of metal ion release and delayed endothelialization pertinent to bare metallic stents.

Acknowledgements

The authors gratefully acknowledge the Department of Biotechnology, Government of India, for financial assistance through a project grant under the Bioengineering Task Force. One of the authors (AP) also acknowledges Department of Science and Technology, Government of India for financial assistance under the M.Tech project grant "PG Training Programs (M.Tech Nanomedical Science) SR/NM/PG-02/08. The authors also thank Mr. Sajin P Ravi and Mr S Sarath for their help with SEM, XRD and XPS analyses and Dr. Dhamodaran Santhanagopalan for invaluable discussions. SAIF, IIT Mumbai and SAIF, CUSAT are also acknowledged for their help with nanoindentation, nanoscratch and ICP analysis respectively. Amrita Vishwa Vidyapeetham is acknowledged for providing all infrastructural support for the research work.

Notes and references

^aAmrita Centre for Nanosciences, Amrita Institute of Medical Science and Research Centre, Amrita Vishwa Vidyapeetham, Cochin-682 041, Kerala, India

*Corresponding author: deephymenon@aims.amrita.edu; deepsmenon@gmail.com

† Both authors contributed equally

1. M. Navarro, A. Michiardi, O. Castano and J.A Planell, *J. R. Soc. Interface*, 2008, **5**, 1137.
2. J. Walczak, F. Shahgaldi and F. Heatley, *Biomaterials*, 1998, **19**, 229.
3. D. O. Halwani, P. G. Anderson, J. E. Lemons and W. D. Jordan, *J. Invasive Cardiol.*, 2010, **22**, 528.
4. D.O. Halwani. PhD thesis, University of Alabama, 2010.
5. S. Windecker, I. Mayer and G. D. Pasquale, *Circulation*, 2001, **104**, 928.

6. G. Manivasagam, D. Dhinasekaran and A. Rajamanickam, *Recent. Pat. Corros. Sci.*, 2010, **2**, 40.
7. V. Gupta, B. R. Aravamuthan, S. Baskerville and S. K. Smith, *J. Invasive. Cardiol.*, 2004, **16**, 304.
8. J. A. Ormiston and P. W. S. Serrus, *Circ. Cardiovasc. Interv.*, 2009, **2**, 255-60.
9. G. G. Stefanini and D. R. Holmes, *N. Engl. J. Med.*, 2013, **368**, 254.
10. A. L. Lewis, J. D. Furze, S. Small and J.D Robertson, *J. Biomed. Mater. Res.*, 2002, **63**, 699.
11. B. Heublein, R. Rohde, V. Kaese and M. Niemeyer, *Heart*, 2003, **89**, 651.
12. R. Zeng, W. Dietzel, F. Witte, N. Hort, C. Blawert, *Adv. Eng. Mater.*, 2008, **10**, B3.
13. A.K.Mitra, D. K. Agrawal, *J. Clin. Pathol.*, 2006, **59**, 232.
14. W. Khan, S. Farah, A. J. Domb, *J. Control. Release*, 2012, **161**, 703.
15. R. Virmani, G. Guagliumi, A. Farb and G. Musumeci, *Circulation*, 2004, **109**, 701.
16. G. S. Was, J.D. Demaree, V. Rotberg and K.Kim, *Surf. Coat. Tech.* 1994, **66**, 446.
17. K. Feng, X. Cai, Z. Li and P. K. Chu, *Mater. Lett.*, 2012, **68**, 450.
18. R. M. Streicher, M. Schmidt and S. Fiorito, *Nanomedicine*, 2007, **2**, 861.
19. C.C Mohan, P. R. Sreerexha, V. V. Divyarani, S. V. Nair, K. P. Chennazhi and D. Menon, *J. Mater. Chem.*, 2012, **22**, 1326.
20. V. V. Divya Rani, K. Manzoor, D. Menon, N. Selvamurugan and S. V. Nair, *Nanotechnology*, 2009, **20**, 195101.
21. V. V. Divya Rani, K. L. Vinoth, V. C. Anitha, K. Manzoor, D. Menon and S. V. Nair, *Acta. Biomater.*, 2012, **8**, 1976.
22. X. Y. Wang and D. Y. Li, *Electrochim. Acta.*, 2002, **47**, 3939.
23. W. G. Kim and H.C. Choe, *T. Nonferr. Metal. Soc.*, 2009, **19**, 1005.
24. X. Y. Zhang, M. H. Shi, C. Li, N. F. Liu, Y. M. Wei, *Mater. Sci. Eng. A*, 2007, **448**, 259.
25. A. R. Cano, M. A. P. Olivenza, R. Babiano, P. Cintas and M. L. G. Martin, *Surf. Coat. Tech.*, 2014, **245**, 66.
26. M. Barbu, M. Stoia and O. Stefanescu, *Chem. Bull. Politehnica*, 2010, **55**, 180.
27. I. H. Toor, *J. Chem.*, 2014, 1–8.
28. Treatise of Material Science and Technology: Corrosion: Aqueous Processes and Passive Films, ed. J. Scully, Academic Press, New York, 1983.
29. M. Mikulewicz, K. Chojnacka and P. Downarowicz, *Biol. Trace. Elem. Res.*, 2012, **146**, 272.
30. G. M. Pharr and W. C. Oliver, *M.R.S. Bulletin*, 1992, **17**, 28.
31. A. Leice, Y. Dekhtyar and N. Britzina, *Environ. Exp. Bio.*, 2010, **8**, 107.
32. E. A. Jaffe, R. L. Nachman, C. G. Becker and C. R. Minick, *J. Clin. Invest.*, 1973, **52**, 2745.
33. A. Testino, V. Buscaglia, M. T. Buscaglia, M. Viviani and P. Nanni, *Chem. Mater.*, 2005, **17**, 5346.
34. M. Chemkhia, D. Retrainta, A. Roosa, C. Garniera, L. Waltzb, C. Demangele and G. Proustd, *Surf. Coat. Tech.*, 2013, **221**, 191.
35. R. Natarajan, N. Palaniswamy and M. Natesan, *Corr. J.*, 2009, **2**, 114.
36. S. J. Yuan, F. J. Xu, S. O. Pehkonen, Y. P. Ting, E. T. Kang and K. G. Neoha, *J. Electrochem. Soc.*, 2008, **155**, C196.
37. A. P. Grosvenor, M. C. Biesinger, S. Roger and N. S. McIntyre, *Surf. Sci.*, 2006, **600**, 1771.
38. T. Hanawa, S. Hiromoto and A. Yamamoto, *Mater. Trans.*, 2002, **43**, 3088-92.
39. H. Wanga and J. A. Turnera, *ECS. Trans.*, 2006, **1**, 263.
40. N. Sato, *J. Electrochem. Soc.*, 1982, **129**, 255.
41. C. Bauer and W. Wuillemin, *Compr. Hum. Physiol.*, 1996, 1651-77.
42. C. C. Mohan, K. P. Chennazhi and D. Menon, *Acta. Biomater.*, 2013, **9**, 9568.
43. B. K. K. Teo, S. T. Wong, C. K. Lim, T. Y. S. Kung, C. H. Yap, Y. Ramagopal, L. H. Romer and E. K. F. Yim, *ACS Nano*, 2013, **7**, 4785.
44. A. B. Bloom and M. H. Zaman, *Physiol. Genomics*, 2014, **46**, 309.
45. H. Ceylan, A. B. Tekinay and M. O. Guler, *Biomaterials*, 2011, **32**, 8797.
46. J. Lu, M. P. Rao, N. C. MacDonald, D. Khang and T. J. Webster, *Acta. Biomater.*, 2008, **4**, 192.
47. L. Peng, M. L. Eltgroth, T. J. La Tempa, C. A. Grimes and T. A. Desai, *Biomaterials*, 2009, **30**, 1268.
48. G. Mani, M. D. Feldman, D. Patel and C. M. Agrawal, *Biomaterials*, 2007, **28**, 1689.
49. J. D. Pearson, *Lupus*, 2000, **9**, 183.
50. J. Lu, M. P. Rao, N. C. MacDonald, D. Khang and T. J. Webster, *Acta. Biomater.*, 2008, **4**, 192.